Immotile Active Matter: Activity from Death and Reproduction

Arben Kalziqi,[1] David Yanni,[1] Jacob Thomas,[2] Siu Lung Ng,[2] Skanda Vivek,[1]
Brian K. Hammer,[2] and Peter J. Yunker[1]
[1]School of Physics, Georgia Institute of Technology, Atlanta, Georgia 30332, USA
[2]School of Biological Sciences, Georgia Institute of Technology, Atlanta, Georgia 30332, USA

(Received 11 February 2017; revised manuscript received 24 July 2017; published 5 January 2018)

Unlike equilibrium atomic solids, biofilms—soft solids composed of bacterial cells—do not experience significant thermal fluctuations at the constituent level. However, living cells stochastically reproduce and die, provoking a mechanical response. We investigate the mechanical consequences of cellular death and reproduction by measuring surface-height fluctuations of biofilms containing two mutually antagonistic strains of *Vibrio cholerae* that kill one another on contact via the type VI secretion system. While studies of active matter typically focus on activity via constituent mobility, here, activity is mediated by reproduction and death events in otherwise immobilized cells. Biofilm surface topography is measured in the nearly homeostatic limit via white light interferometry. Although biofilms are far from equilibrium systems, measured surface-height fluctuation spectra resemble the spectra of thermal permeable membranes but with an activity-mediated effective temperature, as predicted by Risler, Peilloux, and Prost [Phys. Rev. Lett. **115**, 258104 (2015)]. By comparing the activity of killer strains of *V. cholerae* with that of genetically modified strains that cannot kill each other and validating with individual-based simulations, we demonstrate that extracted effective temperatures increase with the amount of death and reproduction and that death and reproduction can fluidize biofilms. Together, these observations demonstrate the unique physical consequences of activity mediated by death and reproduction events.

DOI: 10.1103/PhysRevLett.120.018101

Unlike nonliving matter, living cells are active: They consume energy and exist far from equilibrium. Densely packed cells form solids, much like nonliving matter, but activity at the constituent level gives rise to new phenomena. Although the study of active matter has primarily focused on activity via constituent mobility—in phenomena ranging from spontaneous flocking to a density-independent fluid-to-glass transition in tissues [1–8]—activity can also arise in living systems due to fluctuations in the constituent number, i.e., cellular reproduction and death. Theoretical investigations of apoptosis and reproduction in tissues [9–12] suggest that fluctuations in the cell number may have a fluidizing effect. In fact, exact analytical relations calculated by Risler, Peilloux, and Prost [9] demonstrate that stochastic fluctuations in the constituent number may have observable consequences on the tissue's surface. Specifically, in the low-frequency, long-wavelength limit, they predict that surface-height fluctuations exhibit a spectral structure similar to that of a thermal permeable membrane, with an activity-mediated effective temperature [9]. The experimental observation of this phenomenon would help elucidate the role that nonequilibrium statistical physics can play in the behavior of biological solids, wherein constituent death is unavoidable. However, controlled experiments probing this phenomenon remain elusive, as it is difficult to tune cell reproduction and death rates without inadvertently changing other cellular processes. Furthermore, such effects can be obscured or mitigated by the presence of the extracellular matrix [13], and very high out-of-plane resolution is required to compare experiments with theoretical predictions (see Sec. 10 of Supplemental Material [14]).

Bacterial biofilms represent a natural model system to experimentally investigate the effects of fluctuations in the constituent number. Because of their overwhelming prevalence, as well as ecological, medical, and environmental impact [15–24], these densely packed, surface-attached communities have been the subject of many experimental and theoretical works focusing on their mechanical properties [13,25–27]. Here, biofilms function as soft solids wherein cells act as building blocks, much like atoms or colloidal particles. However, unlike nonliving matter, bacteria can reproduce and die; as a result, the constituent number is not strictly conserved. Furthermore, the genetic manipulation of many bacteria—e.g., *Vibrio cholerae*—is quite advanced, permitting the construction of strains for carefully controlled experiments. Much as colloidal particles act as chemically modifiable model atoms, these bacteria can serve as genetically modifiable model "active atoms".

To elucidate the role that cell death and reproduction play in the structure and mechanics of biofilms, we use *Vibrio cholerae*; the amenability of *V. cholerae* to genetic manipulation makes it well suited for use as a model system. We utilize two newly constructed isogenic "mutual killer" strains of *V. cholerae* (SN306 and SN316) which differ only in the toxic effector used to kill the other strain. We also study genetically modified "nonkiller" strains (SN311 and SN318)

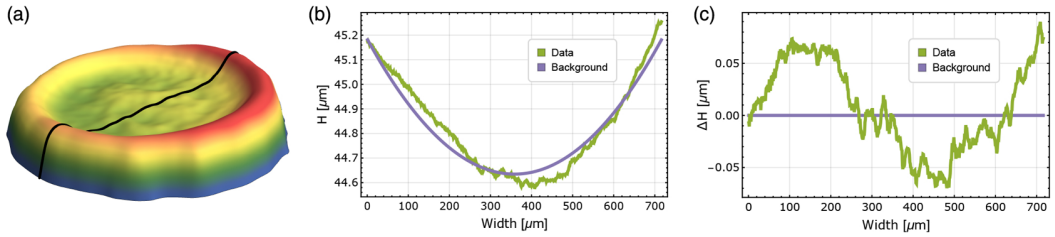

FIG. 1. (a) A 3D profile of a *V. cholerae* biofilm measured via white light interferometry. (b) Profile of a 2D slice of the homeland of the biofilm from (a) (indicated by the green line) superimposed onto the best-fit ellipsoidal background. (c) The biofilm profile with the ellipsoidal background subtracted.

which cannot kill but are otherwise identical to the mutual killers [28,29]. All four strains are genetically modified to produce no extracellular polymeric substances [30], resulting in biofilms that lack internal voids, and have structures resembling stacks of cells sitting on an agar surface (see Sec. 6 of Ref. [14] for more details). The derivative strains are also engineered to express either the Kusabira Orange (mKO) orange fluorescent protein (SN306 and SN311) or the teal fluorescent protein (SN316 and SN318) for microscopy. The transverse size of the biofilm is measured with nanometer precision out of plane with white light interferometry (ZYGO NewView 8300). Height spatial correlation functions are calculated and found to be consistent with predictions by Risler, Peilloux, and Prost [9], permitting us to extract activity-mediated effective temperatures. We find that contact killing increases the average effective temperature by a factor of ∼17.7. By experimentally measuring the motion of tracer beads and simulating the motion of cells in biofilms, we observe that biofilms without killing experience a long-lived jammed state, whereas with killing, biofilms are rapidly fluidized [10–12]. Individual-based simulations demonstrate that cell death significantly mobilizes cells, even at distances many cell lengths away from killing events. Thus, activity via changes in the constituent number significantly alters the properties of active solids in a way that would not be possible with nonliving solids or living solids whose activity is derived from constituent mobility.

To investigate the role of death- and reproduction-mediated activity, we prepare biofilms with varying levels of activity. We deposit 1 μL of inoculum containing about 8×10^5 cells directly onto a nutrient-rich lysogeny broth agar gel; biofilms then grow at the solid-air interface. Inocula were prepared from overnight shaking cultures and contained the two mutually antagonistic *V. cholerae* strains in ratios of 1:1.4; nonkillers were inoculated at a ratio of 1:1.4 as well (see Sec. 1 of Ref. [14] for more details). The mutual killer strains kill each other on contact via the type VI secretion system (T6SS), a microbial warfare mechanism by which bacteria can selectively kill neighboring competitors by injecting them with toxic effectors delivered via a protein spike [31]. The nonkiller strains are identical to the mutual killer strains, except they lack an enzyme essential for the assembly of the T6SS spike. Each biofilm colony was then incubated at 37 °C for 24 h. We incubated 18 samples each for mutual killer and nonkiller strains, on four separate agar plates. The resulting biofilms are shaped like spherical caps with a concave, slightly ellipsoidal dimple [Fig. 1(a)], which arises from the coffee-ring-derived density profile at inoculation. After incubation, we measured the surface-height profiles within the center of each colony's "homeland"—i.e., the disk whose boundary is defined by the initial inoculation ring—with a ZYGO NewView 8000 interferometer. To focus on local fluctuations in the height, rather than the macroscopic shape, an ellipsoidal background was fit to and subtracted from each of the measured surfaces (Fig. 1) (see Sec. 3 of [14]).

For each sample, we calculated an unnormalized equal-time two-point height correlation function $C(\boldsymbol{r}-\boldsymbol{r}') = \langle \Delta H(\boldsymbol{r}, t=0)\Delta H(\boldsymbol{r}', t=0)\rangle$ with the median height set to 0 m. Our scans have a lateral resolution of ∼500 nm—about one-quarter of a cell length—and a vertical resolution of ∼1 nm. Nonkiller biofilms appear visibly smoother than mutual killer biofilms [Fig. 2(c)].

To directly compare to surface fluctuation predictions [9], we calculate the real part of the Fourier transform of the height correlation function. Specifically, the leading term of this Fourier transform is predicted, in the low-q limit, to be $C(q) = [k_B T_{\text{eff}}/(\gamma q^2 + \kappa q^4)]$, where k_B is Boltzmann's constant, γ is the surface tension, κ is the bending rigidity, and q is the wave number. Independent mechanical measurements performed as described in Ref. [32] show $\gamma = 0.023 \pm 0.004\ \text{N m}^{-1}$ and $\kappa = 3.4 \pm 0.5 \times 10^{-11}\ \text{Pa m}^3$ uniformly across samples (for more information, see Sec. 2 of [14]). All examined samples exhibit a q^{-2} regime at small q. Note that this functional form of $C(q)$ is predicted to hold in the low-wave-number regime ($qH \ll 1$; for our biofilms, $H = 45.0 \pm 7.5\ \mu$m) [9]; interestingly, we find that it accurately describes the data up to larger q values than expected (see Secs. 8 and 9 of [14]).

Next, we extract an effective temperature for each of the profiled biofilms [Fig. 2(b); see Secs. 7 and 8 of [14] for details]. Because the nonkiller strains cannot kill, those samples establish a baseline level of activity—and thus a baseline effective temperature—against which the mutual killer samples were compared. For mutual killer biofilms $T_{\text{eff}} = 7.83 \pm 4.99 \times 10^7$ K, while for nonkiller biofilms $T_{\text{eff}} = 4.43 \pm 2.64 \times 10^6$ K (temperatures reported with

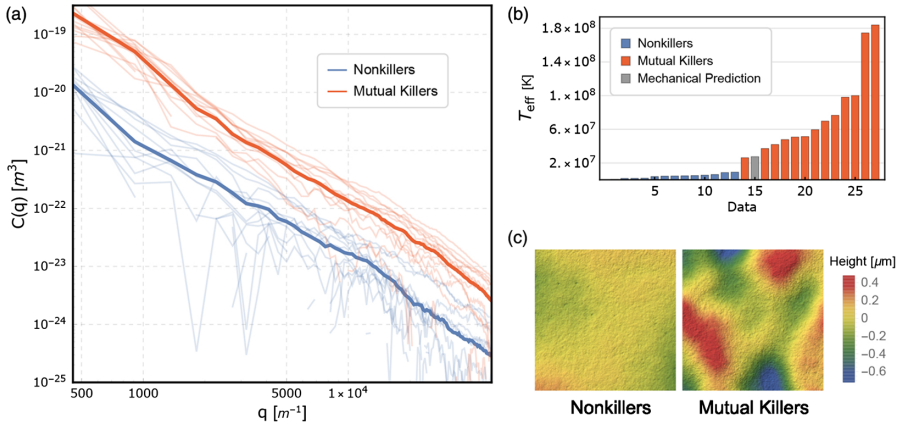

FIG. 2. (a) A log-log plot of the Fourier transformed correlation functions $C(q)$, obtained via interferometry, shown as faint blue (nonkiller) and faint red (mutual killer) lines. Full-opacity lines are averages over 13 nonkiller samples and 13 mutual killer samples. (b) A bar plot of all extracted effective temperatures for nonkiller and mutual killer biofilms. Nonkillers and mutual killers are entirely separated from one another. The mechanically predicted T_{eff} is shown in gray. (c) Selected surface relief plots of the homelands of nonkiller biofilms and mutual killer biofilms. The mutual killer biofilm topographies are all "rougher" than their nonkiller counterparts. Each relief plot is 700×700 μm. See Supplemental Material for all relief plots (Sec. 4 of [14]).

standard deviation; a one-tailed t test shows that samples with killing are significantly different than those without [$p = 1.75 \times 10^{-4}$]).

To corroborate our measurements of T_{eff}, we compare to a zero-free-parameter estimate. To leading order, $T_{\mathrm{eff}} = (\eta r/k_B n)$, where k_B is Boltzmann's constant, η is the bulk viscosity, r is the reproduction rate, and n is the number density [9]. Independent measurements of these parameters (cf. Sec. 2 of [14]) place the predicted T_{eff} in line with the correlation functions extracted by surface metrology for mutual killer biofilms [Fig. 2(a)]. While the agreement between this estimate and our data is quite good, that they are of the same order of magnitude suggests that this model [9] has included the most relevant interactions and parameters.

The agreement between these results and the model in [9] is surprising, in part because of differences in the source and distribution of cell death. While Risler, Peilloux, and Prost [9] model random death in tissues, here, killing occurs only at interfaces between the two bacterial strains (cf. Sec. 5 of [14]). To understand how contact killing at interfaces affects individual cells, we developed an individual-based model of the biofilm [33] (see Sec. 11 of [14] for more details). The model is a physically motivated, biologically minimal framework that focuses on the active matter aspects of biological solids. Member cells interact mechanically as repelling, elastic spheres embedded in a viscous medium as described in [34]. Cells undergo growth, division, and death but are otherwise biologically inert. Death can be induced by interstrain contact killing or can occur naturally. These simulations recapitulate the qualitative and quantitative results of the experiments. Simulating biofilms with high levels of contact killing produces surface topographies that appear qualitatively similar to mutual killer biofilms (see Sec. 4 of [14]), while simulating biofilms with very low levels of killing produces surface topographies that appear qualitatively similar to nonkiller biofilms (see Sec. 4 of [14]). Amplitudes of extracted correlation functions vary with the killing rate, as expected [9] (see Sec. 9 of [14]).

We next investigated the dynamics of individual cells via simulations with no death, simulations with random cell death, and simulations of mutual killers with random cell death [Fig. 3(c)]. In each case, we measure the mean-squared displacement $\Delta r^2(\Delta t) = \langle \sum_i [x_{ij}(t) - x_{ij}(t+\Delta t)]^2 \rangle_j$, where x_{ij} represents the ith coordinate of cell j, Δt is the lag time, the sum $\sum_i$ extends over all coordinates i, $\langle \rangle_j$ indicates an average over different cells, and Δr^2 is the mean-squared displacement [Fig. 3(a)]. Cells in simulations absent death have flat Δr^2 curves, indicating that cells remain caged by their neighbors in a long-lived jammed state. Cells in simulations with random cell death have Δr^2 curves that are initially flat before an upturn to a linear increase in Δr^2 versus Δt. This indicates that, while cells are caged over short time periods, they eventually break their cages and move diffusively, as suggested in previous theoretical works [1–4,10,11]. "Mutual killer" cells (i.e., cells that experience random death and engage in killing) have Δr^2 curves that are similar to the random death Δr^2 curves, suggesting that contact killing fluidizes biofilms in a manner similar to random cell death [Figs. 3(a) and 3(b)] [12].

To investigate how contact killing affects cells that are not at the interface between strains, we simulated biofilms with intercellular killing only (no random death) at a single killing interface and measured Δr^2 curves for cells at different distances from that interface [Fig. 3(b)]. We find that the Δr^2 grows linearly with Δt for cells at any distance from the interface, though the upturn in the Δr^2 from caged to diffusive occurs at longer values of Δt for cells farther from the interface. It may initially appear surprising that death localized at an interface can dramatically affect the

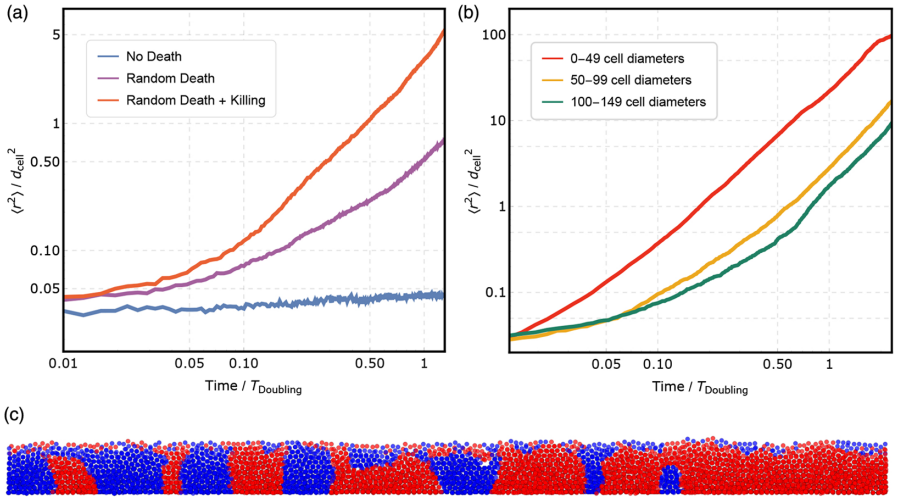

FIG. 3. (a) A log-log plot of the mean-squared displacement (measured in cell diameters^2) of cells in simulated biofilms with no death, with only random death, and with both random death and killing (cf. mutual killer biofilms). Nonkiller biofilms have a low level of cell death but do not exactly correspond to any of the three presented curves. The addition of intercellular killing significantly mobilizes the cells inside the biofilm, fluidizing it. (b) A log-log plot of average cellular mean-squared displacements for bins of cells at various distances from killing interfaces. Closer to these interfaces, cells are significantly more mobile. (c) A simulated mutual killer biofilm with the two mutual killer strains shown in different colors. See Fig. S2 for comparative relief maps of simulated biofilms with low killing and high killing in the style of Fig. 2(c).

cell mobility far from the interface. However, this is consistent with the predictions of Refs. [9,10,35]; apoptosis and reproduction are intrinsically local, and yet they can hold mechanical consequences over long distances.

Unfortunately, individual cells cannot be directly imaged in our experiments. Thus, to provide an experimentally testable measure of biofilm fluidization from death and reproduction, we simulate biofilms with tracer beads, which do not reproduce, kill, or die. We also allow reproduction to occur only within a distance of 5% of the total biofilm height from the bottom layer of the biofilm [36] (see Sec. 12 of [14] for more details). This better replicates the behavior of biofilms grown on agar, where nutrients come from below, permitting us to generate testable qualitative predictions. We observe that simulating contact killing or random death causes tracer beads to move up towards the biofilm's top surface over time and that higher rates of death and reproduction cause the beads to move to the top surface faster. There is no net upward movement of tracer beads in control simulations of nonkillers absent death.

To experimentally test this prediction, we insert 1-μm-diameter tracer beads (Bangs Labs) into biofilms and image their locations 13 and 26 h after inoculation (see Sec. 13 of [14] for more information). Specifically, we measured the fraction of beads that are in the top third of the biofilm, i.e., the fraction of beads that are within 15 μm of the top biofilm surface. For nonkiller biofilms, the fraction of beads near the surface increased from 0.19 ± 0.04 to

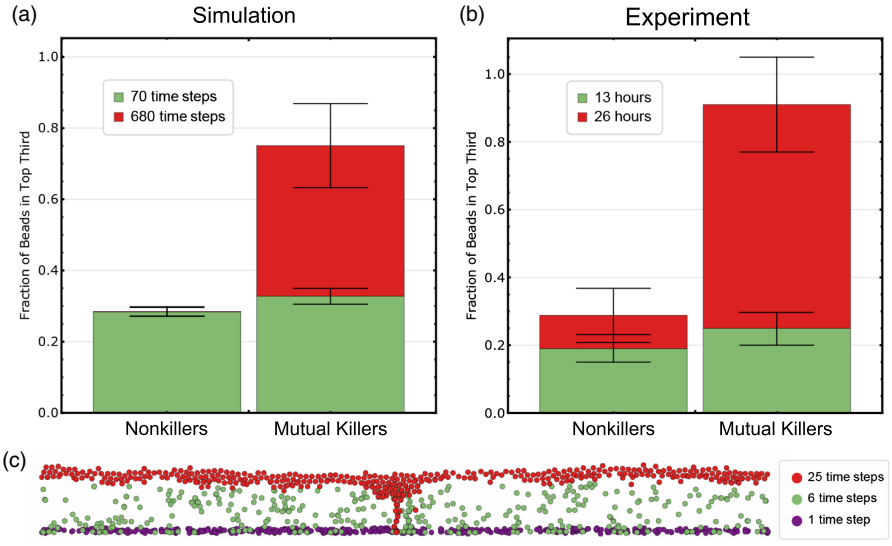

FIG. 4. (a) Simulated biofilms with no death show little change in the tracer bead position over time, but simulated mutual killer biofilms exhibit behavior consistent with that of a convective medium, as seen in cellular aggregates with cell division and death [37,38]. (b) In experiments, tracer beads are convected toward the top third of nonkiller biofilms over time, but mutual killer biofilms are significantly more convective, allowing for nearly all of the tracer beads to move to the top. (c) The positions of tracer beads in a simulated mutual killer biofilm are shown at initialization, at an intermediate time, and at a late time. Tracer beads rapidly leave their initial positions and settle at the biofilm top surface.

0.29 ± 0.08. Remarkably, for mutual killer biofilms, the fraction of beads near the surface increased from 0.25 ± 0.05 to 0.91 ± 0.14. The bead distributions are statistically similar at 13 h (two-tailed t test, $p = 0.327$), whereas at 26 h, the bead distributions are significantly different (two-tailed t test, $p = 0.006$). Thus, the tracer beads in the mutual killer biofilms are much more mobile than the tracer beads in the nonkiller biofilms (Fig. 4).

The presence of a quantitative relationship between surface topography and cell death opens new avenues for studying both physical and biological properties of biofilms. Just as measuring fluctuations in equilibrium materials permits the calculation of mechanical response functions [39], mechanical and structural measurements of biofilms and tissues can be used to infer death and reproduction rates—quantities that are difficult to measure in densely packed cellular solids. However, further work is necessary to ascertain if the approach employed here would work in biofilms with substantial viscoelastic extracellular matrix secretions [40]. Furthermore, along with other recent results [41–43], the observations reported here support the idea that death and reproduction have a fluidizing effect [1–4,9–12] and suggest that a statistical description of biofilms, rooted in the extension of concepts from equilibrium statistical mechanics [44–46], may yet play a large role in explaining complex microbial communities. Finally, it is surprising that the biofilms studied here exhibit an apparent universality in surface fluctuation spectra with thermal permeable membranes, as well as nonequilibrium tissues [9], despite many differences in these systems.

This work was supported by NSF Grant No. IOS-1656549 to P. J. Y., the Gordon and Betty Moore Foundation Grant No. 4308.07 to B. K. H., and NSF Grant No. MCB-1149925 to B. K. H. We would like to thank William Ratcliff and Daniel Goldman for helpful comments.

[1] D. Bi, J. H. Lopez, J. M. Schwartz, and L. Manning, A density-independent rigidity transition in biological tissues, Nat. Phys. **11**, 1074 (2015).
[2] M. C. Marchetti, J. F. Joanny, S. Ramaswamy, T. B. Liverpool, J. R. M. Prost, and R. A. Simha, Hydrodynamics of soft active matter, Rev. Mod. Phys. **85**, 1143 (2013).
[3] A. Tribocchi, R. Wittkowski, D. Marenduzzo, and M. E. Cates, Active Model H: Scalar Active Matter in a Momentum-Conserving Fluid, Phys. Rev. Lett. **115**, 188302 (2015).
[4] C. A. Weber, C. Bock, and E. Frey, Defect-Mediated Phase Transitions in Active Soft Matter, Phys. Rev. Lett. **112**, 168301 (2014).
[5] C. Peng, T. Turiv, Y. Guo, Q.-H. Wei, and O. D. Lavrentovich, Command of active matter by topological defects and patterns, Science **354**, 882 (2016).
[6] J. L. Silverberg, M. Bierbaum, J. P. Sethna, and I. Cohen, Collective Motion of Humans in Mosh and Circle Pits at Heavy Metal Concerts, Phys. Rev. Lett. **110**, 228701 (2013).
[7] M. E. Cates and J. Tailleur, Motility-induced phase separation, Annu. Rev. Condens. Matter Phys. **6**, 219 (2015).
[8] T. Sanchez, D. T. Chen, S. J. Decamp, M. Heymann, and Z. Dogic, Spontaneous motion in hierarchically assembled active matter, Nature (London) **491**, 431 (2012).
[9] T. Risler, A. Peilloux, and J. Prost, Homeostatic Fluctuations of a Tissue Surface, Phys. Rev. Lett. **115**, 258104 (2015).
[10] J. Ranft, M. Basan, J. Elgeti, J.-F. Joanny, J. Prost, and F. Jülicher, Fluidization of tissues by cell division and apoptosis, Proc. Natl. Acad. Sci. U.S.A. **107**, 20863 (2010).
[11] D. A. Matoz-Fernandez, K. Martens, R. Sknepnek, J. L. Barrat, and S. Henkes, Cell division and death inhibit glassy behaviour of confluent tissues, Soft Matter **13**, 3205 (2017).
[12] M. Basan, J. Prost, J.-F. Joanny, and J. Elgeti, Dissipative particle dynamics simulations for biological tissues: Rheology and competition, Phys. Biol. **8**, 026014 (2011).
[13] C. A. Rodesney, B. Roman, N. Dhamani, B. J. Cooley, P. Katira, A. Touhami, and V. D. Gordon, Mechanosensing of shear by Pseudomonas aeruginosa leads to increased levels of the cyclic-di-GMP signal initiating biofilm development, Proc. Natl. Acad. Sci. U.S.A. **114**, 5906 (2017).
[14] See Supplemental Material at http://link.aps.org/supplemental/10.1103/PhysRevLett.120.018101 for details regarding biofilm inoculation, internal structure, measurement, and simulation.
[15] P. Watnick and R. Kolter, Biofilm, city of microbes, J. Bacteriol. **182**, 2675 (2000).
[16] V. Zijnge, M. B. M. van Leeuwen, J. E. Degener, F. Abbas, T. Thumheer, and R. H. H. J. M. Gmür, Oral biofilm architecture on natural teeth, PLoS One **5**, e9321 (2010).
[17] S. Macfarlane and J. Dillon, Microbial biofilms in the human gastrointestinal tract, J. Appl. Microbiol. **102**, 1187 (2007).
[18] T.-F. C. Mah and G. A. O'Toole, Mechanisms of biofilm resistance to antimicrobial agents, Trends Microbiol. **9**, 34 (2001).
[19] J. Costerton, L. Montanaro, and C. Arciola, Biofilm in implant infections: Its production and regulation, Int. J. Artif. Organs **28**, 1062 (2005).
[20] J. L. Balcázar, J. Subirats, and C. M. Borrego, The role of biofilms as environmental reservoirs of antibiotic resistance, Front. Microbiol. **6**, 1216 (2015).
[21] M. Ledin and K. Perderson, The environmental impact of mine wastes—Roles of microorganisms and their significance in treatment of mine wastes, Earth-Sci. Rev. **41**, 67 (1996).
[22] C. Säwström, P. Mumford, W. Marshall, A. Hodson, and J. Laybourn-Parry, The microbial communities and primary productivity of cryoconite holes in an Arctic glacier (Svalbard 79°N), Polar Biol. **25**, 591 (2002).
[23] C. E. Morris and J.-M. Monier, The ecological significance of biofilm formation by plant-associated bacteria, Annu. Rev. Phytopathol. **41**, 429 (2003).
[24] C. Matz, D. McDougald, A. M. Moreno, P. Y. Yung, F. H. Yildiz, and S. Kjelleberg, Biofilm formation and phenotypic variation enhance predation-driven persistence of Vibrio cholerae, Proc. Natl. Acad. Sci. U.S.A. **102**, 16819 (2005).
[25] J. N. Wilking, T. E. Angelini, A. Seminara, and M. P. Brenner, Biofilms as complex fluids, MRS Bull. **36**, 385 (2011).
[26] A. Persat, C. D. Nadell, M. K. Kim, F. Ingremeau, A. Siryaporn, K. Drescher, N. S. Wingreen, B. L. Bassler,

Z. Gitai, and H. A. Stone, The mechanical world of bacteria, Cell **161**, 988 (2015).
[27] M. G. Mazza, The physics of biofilms—An introduction, J. Phys. D **49**, 203001 (2016).
[28] J. Thomas, S. S. Watve, W. C. Ratcliff, and B. K. Hammer, Horizontal gene transfer of functional type VI killing genes by natural transformation, mBio **8**, e00654-17 (2017).
[29] S. S. Watve, J. Thomas, and B. K. Hammer, CytR is a global positive regulator of competence, type VI secretion, and chitinases in Vibrio cholerae, PLoS One **10**, e0138834 (2015).
[30] B. K. Hammer and B. L. Bassler, Quorum sensing controls biofilm formation in Vibrio cholerae, Mol. Microbiol. **50**, 101 (2003).
[31] D. L. MacIntyre, S. T. Miyata, M. Kitaoka, and S. Pukatzki, The Vibrio cholerae type VI secretion system displays antimicrobial properties, Proc. Natl. Acad. Sci. U.S.A. **107**, 19520 (2010).
[32] G. Forgacs, R. A. Foty, Y. Shafrir, and M. S. Steinberg, Viscoelastic properties of living embryonic tissues: A quantitative study, Biophys. J. **74**, 2227 (1998).
[33] G. W. Jones and S. J. Chapman, Modeling growth in biological materials, SIAM Rev. **54**, 52 (2012).
[34] J.-U. Kreft, C. Picioreanu, J. W. T. Wimpenny, and M. C. M. van Loosdrecht, Individual-based modelling of biofilms, Microbiology **147**, 2897 (2001).
[35] M. Delarue, F. Montel, O. Caen, J. Elgeti, J.-M. Siaugue, D. Vignjevic, J. Prost, and J.-F. C. G. Joanny, Mechanical Control of Cell Flow in Multicellular Spheroids, Phys. Rev. Lett. **110**, 138103 (2013).
[36] X. Zhang, X. Wang, K. Nie, M. Li, and Q. Sun, Simulation of Bacillus subtilis biofilm growth on agar plate by diffusion–reaction based continuum model, Phys. Biol. **13**, 046002 (2016).
[37] M. J. Dorie, R. F. Kallman, and M. A. Coyne, Effect of cytochalasin B, nocodazole and irradiation on migration and internalization of cells and microspheres in tumor cell spheroids, Exp. Cell Res. **166**, 370 (1986).
[38] M. J. Dorie, R. F. Kallman, D. V. A. Repacchietta, and Y. R. Huang, Migration and internalization of cells and polystyrene microspheres in tumor cell spheroids, Exp. Cell Res. **141**, 201 (1982).
[39] Y. L. Klimontovich, in *Turbulent Motion and the Structure of Chaos: A New Approach to the Statistical Theory of Open Systems* (Springer, Dordrecht, 1991), Vol. 42, p. 135.
[40] H.-C. Flemming and J. Wingender, The biofilm matrix, Nat. Rev. Microbiol. **8**, 623 (2010).
[41] E. Hernández-Lemus, Nonequilibrium thermodynamics of cell signaling, J. Thermodyn. **2012**, 432143 (2012).
[42] N. Fakhri, A. Wessel, C. Willms, M. Pasquali, D. Klopfenstein, F. MacKintosh, and C. Schmidt, High-resolution mapping of intracellular fluctuations using carbon nanotubes, Science **344**, 1031 (2014).
[43] C. Battle, C. Broedersz, N. Fakhri, V. Geyer, J. Howard, C. Schmidt, and F. MacKintosh, Broken detailed balance at mesoscopic scales in active biological systems, Science **352**, 604 (2016).
[44] L. M. Chen and L. H. Chai, A theoretical analysis on self-organized formation of microbial biofilms, Physica A (Amsterdam) **370**, 793 (2006).
[45] L. McNally, E. Bernardy, J. Thomas, A. Kalziqi, J. Pentz, S. P. Brown, B. K. Hammer, P. J. Yunker, and W. C. Ratcliff, Killing by type VI secretion drives genetic phase separation and correlates with increased cooperation, Nat. Commun. **8**, 14371 (2017).
[46] J. Liu, A. Prindle, J. Humphries, M. Gabalda-Sagarra, M. Asally, D. D. Lee, S. Ly, J. Garcia-Ojalvo, and G. M. Süel, Metabolic co-dependence gives rise to collective oscillations within biofilms, Nature (London) **523**, 550 (2015).